Application of Mean Field Boundary Potentials in Simulations of Lipid Vesicles

H. Jelger Risselada,[†] Alan E. Mark,[†,‡] and Siewert J. Marrink*,[†]

Groningen Biomolecular Sciences and Biotechnology Institute & Zernike Institute for Advanced Materials, University of Groningen, Nijenborgh 4, 9747 AG Groningen, The Netherlands, and School of Molecular and Microbial Sciences and Institute for Molecular Biosciences, University of Queensland, St Lucia, Queensland 4072, Australia

Received: July 25, 2007; Revised Manuscript Received: March 11, 2008

A method is presented to enhance the efficiency of simulations of lipid vesicles. The method increases computational speed by eliminating water molecules that either surround the vesicle or reside in the interior of the vesicle, without altering the properties of the water at the membrane interface. Specifically, mean field force approximation (MFFA) boundary potentials are used to replace both the internal and external excess bulk solvent. In addition to reducing the cost of simulating preformed vesicles, the molding effect of the boundary potentials also enhances the formation and equilibration of vesicles from random solutions of lipid in water. Vesicles with diameters in the range from 20 to 60 nm were obtained on a nanosecond time scale, without any noticeable effect of the boundary potentials on their structure.

1. Introduction

Lipids are small amphiphatic molecules that can adopt a wide variety of aggregation states including micelles, lamellae, and vesicles. In the vesicular state, the lipids form a spherically closed bilayer. Such vesicles, or liposomes, play an important biological role in processes such as endo- and exocytosis and intracellular transport as well as in providing nanoscale reaction vessels. Lipid vesicles are also used in drug delivery applications, and serve as model systems for experimental studies of cell processes. The length scales of vesicular systems in vivo range from nanometers to micrometers (whole cells). In model systems, a similar range in size can be achieved, depending on the type of experimental techniques used. The smallest vesicles are referred to as small unilamellar vesicles (SUVs), whereas the largest, approaching the size of whole cells, are termed giant unilamellar vesicles (GUVs).

A wide variety of computational studies have been performed to understand the behavior of lipid vesicles at the molecular level.[1–12] These studies have been typically based on simplified, coarse grained, lipid models, although processes such as spontaneous vesicle formation and vesicle fusion have even been simulated in full atomistic detail.[13,14] However, due to the computational cost of such calculations, the size of the vesicles that can be considered using present methods is limited to around 20 nm in diameter, close to the minimum size of a vesicle that can be formed experimentally by sonication.[15] Such small vesicles are only marginally stable due the large curvature stresses involved, and simulation studies of fusion between vesicles on this length scale indeed show extremely fast kinetics, with fusion completed on a nano- to microsecond time scale.[5–7,11,16] The effect of curvature is also evident in other measures, such as the melting temperature of the lipids. For pure dipalmitoylphosphatidylcholine (DPPC) vesicles, it is found experimentally that the phase transition temperature decreases with a decrease in the diameter of the vesicle below a threshold of $\simeq$70 nm.[17,18] Such behavior as a function of temperature is also observed for small vesicles in simulations.[19] Although increases in computational power will make it possible to gradually increase the size of vesicles that can be studied in molecular or atomic detail, in order to reach more realistic sizes (exceeding 100 nm), alternative approaches to describe the system are required.

Several methods have been proposed to bridge the gap between detailed atomistic molecular dynamics (MD) simulations and the micrometer lipid vesicles of experimental interest. All methods rely on reducing the number of degrees of freedom and replacing them with mean field descriptors. In the work of Ayton et al.,[20] the physical properties from an atomistic MD study of a PC bilayer were used together with other microscopically determined parameters, to obtain a continuum-level model operating in time and length scales orders of magnitude beyond that which is accessible by atomistic-level simulation. In the work of Sevink et al.,[21] the full kinetic pathways of self-assembly of polymeric amphiphiles into a rich variety of complex vesicles was demonstrated by large-scale computer simulations based on dynamic self-consistent-field theory. Although these methods succeed in describing the system on a micrometer length scale, the approximations made result in the loss of the nanoscopic details of interest. Another solution is to resort to a complete solvent free model. Several groups have successfully demonstrated the formation of vesicles using this approach.[2,3,8–10,22] In principle, such methods allow one to maintain detailed models for the lipid molecules; however, the drawback is that many processes depend directly or indirectly on the explicit presence of water, for example, processes such as pore formation, vesicle deformations, and osmotic swelling. In addition, hydrodynamic interactions are absent in a solvent free approach.

The aim of the method presented in this paper is to bridge toward larger time and length scales, preserving the nanoscopic details, including those of the solvent. We propose the use of a boundary potential which includes explicitly a shell of water around the vesicles but excludes the bulk water present in the vesicle interior or surrounding the vesicle. As most of the computational time of a vesicular system is spent on simulating

* Corresponding author. E-mail: S.J.Marrink@rug.nl.
† University of Groningen.
‡ University of Queensland.

10.1021/jp0758519 CCC: $40.75
Published on Web 05/30/2008

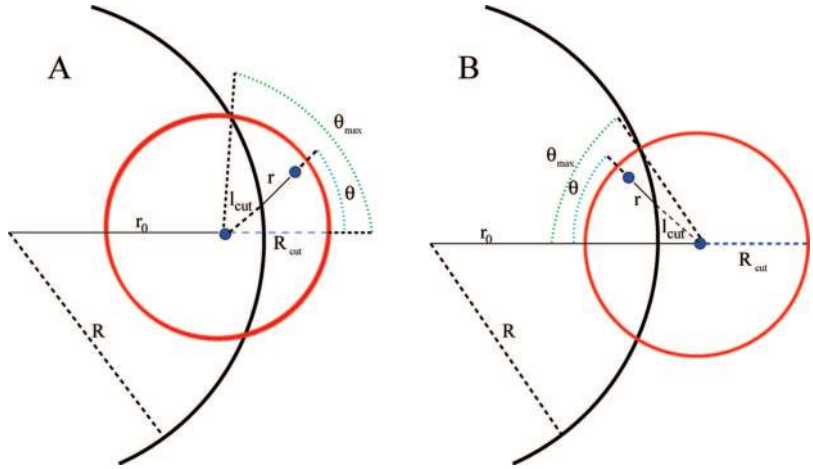

Figure 1. Conceptual picture of the MFFA boundary potential. Shown in part A is the integration scheme for the case where the virtual region is outside the spherical simulation zone. Shown in part B is the case were an internal cavity is present inside the simulation zone. A particle lies within position r_0 from the center of the simulation zone. The particle interacts with a virtual particle outside the simulation at distance r. l_{cut} is the distance between the particle at position r_0 and the point where r intersects with the simulation sphere R. The red sphere depicts the interaction cutoff R_{cut}.

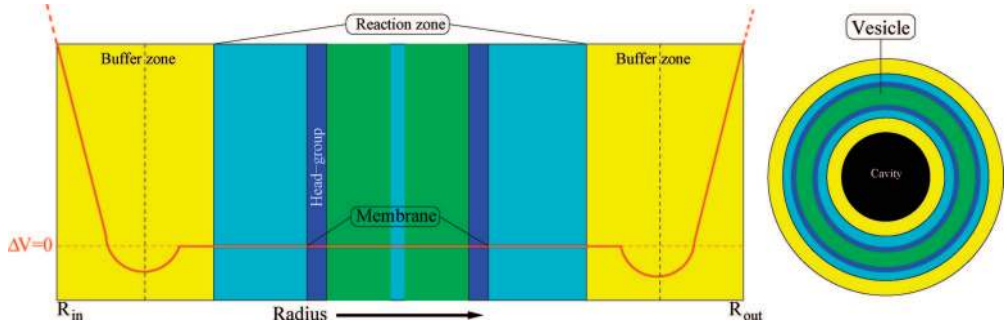

Figure 2. Cartoon depicting the overall simulation setup. The left cartoon shows the cross section of a detailed fragment of the system. The picture on the right shows an overview of the cross section of the entire system, a vesicle under spherical MFFA boundary conditions. The reaction zone contains the membrane and CG water under conventional Newtonian dynamics. In the yellow region, the CG water is subjected to the MFFA boundary potential. The solid red line depicts the MFFA boundary potential. The dashed red line represents the additional harmonic potential which compensates the finite nature of the tabulated MFFA boundary potential beyond the boundaries.

the surrounding and interior water, reducing the water in the system in this way achieves a significant increase in computational efficiency, without losing bulk properties at the membrane interface. The ratio of the accessible volume of the interior water V_{int} inside a vesicle versus the total volume of vesicle V_{tot} scales as

$$\frac{V_{int}}{V_{tot}} \propto \frac{(r-d)^3}{r^3} \tag{1}$$

where r is the radius of a vesicle and d the thickness of the membrane. Equation 1 shows that if the vesicle size is increased, $r \gg d$, the interior water dominates the volume fraction inside the system. As one is interested in processes that occur primarily at or near the vesicular membrane, simulating the bulk water in the interior of the vesicle is unnecessary, as is simulating the excess solvent outside of the vesicle. Given that vesicles are spherical objects, the use of periodic boundary conditions is inefficient, as it requires a simulation box with a space filling geometry. Even in the most efficient unit cell for such a system, the dodecahedron, the solvent is not distributed evenly around the vesicle.[23] Ideally, from a computational point of view, a vesicle could be surrounded by a small water shell on both the inside and the outside of the vesicle, just sufficient to maintain its bulk properties close to the membrane interface.

One method to obtain this is by introducing a solvent boundary potential, which gives a finite representation of an infinite bulk system.[24–26] In the work of Brooks and Karplus,[25] a soft mean field force approximation (MFFA) potential was introduced to represent the interactions of a solvent in the reservoir region on the reaction region. This method did not include the long-range electrostatic corrections due to the polar nature of the surrounding bulk water. Later methods included these electrostatic effects by various approaches.[27–30] However, in all studies cited, it has proved difficult to obtain the isotropic behavior of a solvent near the boundary interface. Especially when electrostatic interactions were involved, like in water, a more anisotropic behavior in both angular and radial distribution functions was observed.

A concern of simulating vesicles within a (spherical) constrained solvent shell is the bias in possible shape undulations c.q. deformations of the vesicle. However, these artifacts are similar to the bias which is introduced by simulating vesicles in a periodic system of similar length scale, where the vesicle feels, either directly or through the solvent, its periodic image. Boundary methods dealing with flexible boundaries have also been introduced. Li et al.[31] presented a fluctuating elastic boundary model which encloses the simulated system in an elastic bag that mimics the effects of the bulk solvent. This boundary bag was modeled as a mesh of quasi-particles connected by elastic bonds, its motions governed by a diffusion equation. Although all shape deformations of the vesicles are possible with such an approach, they are highly affected by the

choise of the elastic bond constants and the diffusion equation which are a priori not known. In practice, the computational expense of solving the equations of motion of these quasi-particle approaches as well as the memory needed for storing the mesh connections scales quadratically with the system size, whereas the computational effort to apply a mean field potential representing the boundary of the system is cheap and independent of the system size.

Here, we apply the MFFA approach of Brooks et al.[25] to minimize the amount of water in both the interior and exterior of the vesicle. This approach has already been successfully used by others in the simulation of small membrane patches.[32,33] The application of this approach in vesicle simulations has never been studied. Our approach has especially been developed for use in conjunction with the coarse grained lipid model of Marrink et al.[34,35] The water in this model is represented simply by Lennard-Jones interactions, lacking any electrostatic interactions or rotational axis. In this case, the boundary potential only represents the mean effect of a pure Lennard-Jones fluid. Complications arising from the integration of long-range electrostatic forces, as with all-atom force fields using Ewald-based summation methods in conjunction with the boundary method, are therefore not present in our model. Likewise, artifacts in the isotropic behavior of the solvent (e.g., rotational ordering at the boundary interface resulting in a net dipole moment[27–30]) do not play a role in the current application.

The aim of the current work is to demonstrate that lipid vesicles can be efficiently simulated using the MFFA boundary approach. The largest vesicle studied here is 60 nm in diameter, triple the size simulated previously in near-atomic detail.[4] Moreover, we show that due to the molding effect of the boundary potentials the process of formation of equilibrated vesicles from initially random lipid solutions is extremely fast (nanosecond time scale). The remainder of the paper is organized as follows. In the next section, the implementation of the boundary potential for vesicular systems is explained along with measures taken to control the temperature and pressure of the system. The methodology is then tested on two systems, namely, a shell of bulk water and a planar lipid membrane. We finally show that the methodology can be applied very efficiently to simulate the formation and subsequent equilibration of a range of vesicles of increasing size.

2. Methods

2.1. The Spherical MFFA Boundary Potential. The approach that is used in this work is analogous to that of Brooks et al.[25] The coordinate system chosen in the original integration scheme presented by Brooks et al, suffers problems with numerical precision when the ratio between the radius of the boundary cutoff R_{cut} and the radius of the spherical boundary R becomes large, which is the case for the systems of interest in this study. Moreover, it should be noted that in the original integration scheme an additional factor of 2 was erroneously introduced, leading to an overestimation of the magnitude of the MFFA potential also by a factor of 2. Here, we present a more robust, alternative way of solving the MFFA potential for any particular water shell of interest.

Consider a spherical system of radius R embedded in an implicit solvent continuum (see Figure 1). The total force on a particle at a distance r_0 from the center of the sphere is due to interactions with all particles within the cutoff sphere R_{cut}. When $r_0 + R_{cut} > R$, part of the volume fraction of the cutoff sphere R_{cut} will be located within the continuum. In this case, the total force on the particle at r_0 is due to the interactions with the explicit particles as well as the interactions with the continuum. The contribution to the total force from the explicit particles within the solvent shell is just the normal sum over pair interactions employed in molecular dynamics. The contribution of the continuum to the total force on the particle at r_0 is given by summing all interactions from all possible positions within the continuum weighted by the probability $\rho g(r)$ of finding an implicit particle at distance r from r_0. Here, ρ is the mean density and $g(r)$ the normalized radial distribution function of the reference solvent. The mean field boundary force from the implicit solvent acting on a particle at r_0 is given by (see Figure 1A)

$$F_w(r_0) = 2\pi \int_0^{\theta_{max}} \sin(\theta)\, d\theta \int_R^{l_{cut}(\theta)} dr\, r^2 \rho g(r)\, F(r) \quad (2)$$

By applying the cosine theorem on the projections in Figure 1, the boundary condition of this convolution integral is solved. The angle θ_{max} is determined from r_0, R, and R_{cut} and gives

$$\theta_{max} = \arccos\left(\frac{R^2 - {r_0}^2 - {R_{cut}}^2}{2 r_0 R_{cut}}\right) \quad (3)$$

The distance l_{cut} is given by

$$l_{cut}(\theta) = -r_0 \cos(\theta) + \sqrt{{r_0}^2 \cos^2(\theta) - {r_0}^2 + R^2} \quad (4)$$

The quantity $F(r)$ is the radial component of the force along the direction $\mathbf{r}_0$, where $\mathbf{r}_0 = (ix_0, iz_0, iy_0)$ is the vector connecting the particle at r_0 and the center of the reaction zone.

$$F(r) = r \cos(\theta)\left(\frac{dV}{dr}\right) \quad (5)$$

with dV/dr denoting the derivative of the pairwise potential interaction function with respect to r. Hence, only its radial component is required due to the azimuthal symmetry around $\mathbf{r}_0$. The overall boundary force $F_w(r_0)$ can be decomposed into its x, y, z components in the reference frame by

$$\mathbf{F}_B(\hat{\mathbf{r}}_0) = \hat{\mathbf{r}}_0 F_w(r_0) \quad (6)$$

where $\hat{\mathbf{r}}_0 = \mathbf{r}_0/r_0$ represents the unit normal vector along r_0. According to the same procedure, the boundary force from the inverted case, where a cavity is surrounded by the simulation zone, can also be obtained (see Figure 1B). In this case, θ_{max} in eq 3 is given by

$$\theta_{max} = \arccos\left(\frac{{R_{cut}}^2 + {r_0}^2 - R^2}{2 r_0 R_{cut}}\right) \quad (7)$$

and $l_{cut}(\theta)$ in eq 4 as

$$l_{cut}(\theta) = r_0 \cos(\theta) - \sqrt{{r_0}^2 \cos^2(\theta) - {r_0}^2 + R^2} \quad (8)$$

A schematic picture of the MFFA boundary potential is given in Figure 2. Particles moving toward the boundary first experience a net attractive force. When particles approach the boundary more closely, they will experience a repulsive force. The strength of this repulsive force is soft in comparison to the normal Lennard-Jones interactions of the solvent. The nature of the mean field force potential is to compensate the surface tension at the boundaries which would otherwise occur in a system having a finite size.

By combining both approaches, any solvent shell of interest, with inner radius R_{in} and outer radius R_{out}, can be obtained. As the MFFA boundary potential is numerically solved and therefore, in practice, a tabulated force potential, it has a finite range. To prevent particles from overcoming the repulsive

barrier of the boundary, an additional repulsive harmonic potential is applied to the particle in the region $r_0 \leq R_{in}$ and $r_0 \geq R_{out}$. The force constant of this harmonic potential is obtained from a linear fit of the repulsive tail region of the tabulated force potential. The MFFA boundary potential method was implemented in the GROMACS-3.3 simulation package.[36]

2.2. Temperature Control. Commonly, when using a MFFA-like boundary, stochastic coupling of the boundaries is used as an external heat bath to maintain constant temperature, e.g., in the EGO simulation software package.[37] However, for the large systems considered in this study, the ratio of surface area to volume meant that the implementation of a stable algorithm for a stochastic boundary zone required either a strong reduction of the integration time step or a much more frequent update of the neighbor pair list to improve energy conservation, compared to the values usually achievable in standard membrane simulations using the CG model.[34] Both of these requirements would render the overall aim of the boundary potential approach, i.e., to improve the computational efficiency of the simulations, ineffective. For this reason, in the applications described in this paper, we use the Berendsen thermostat method,[38] although it should be noted that, strictly speaking, the Berendsen thermostat does not generate a proper NVT/NPT ensemble. In contrast with the Berendsen thermostat, stochastic boundaries include both thermal and density relaxations simultaneously, compensating the sparse nature at the boundaries. As this stochastic effect is missing in the Berendsen thermostat method, there is increased local order near the boundaries, effectively lowering the kinetic barrier of freezing for the solvent near the boundaries. In order to prevent freezing of the CG water near the boundaries in studies where the temperature is close or even lower than the melting temperature of the solvent, a simple solution was adopted. To prevent the development of long-range order and the appearance of a crystal lattice at the boundary interface, so-called antifreeze (AF) particles were introduced.[35] These AF particles interact differently with different particles. For all particles other than the CG water, their interaction is the same as that for CG water. For the interaction between the AF and the CG water, the Lennard-Jones (LJ) parameter σ is changed from 0.47 to 0.57 nm, making the AF particles effectively larger. The optimal packing of the CG water at the boundaries is thus disrupted. A concentration of $\approx$5% of AF particles in the shell is sufficient to prevent the freezing near the boundaries down to temperatures tens of degrees below the freezing point of pure CG water (around 290 K[35]). In section 3.2, we describe results from test runs on bilayers, which showed that the properties of the bilayer were unaffected by the introduction of AF particles.

2.3. Pressure Control. The MFFA boundary potential method provides a system in the NVT ensemble, although the nature of the potential is soft and the effective volume might show small fluctuations. If the method is to be applied to study processes such as vesicle formation or phase transitions where changes in density can occur, the NPT ensemble is more appropriate. In addition, the NPT ensemble allows a better comparison with experiments often performed under atmospheric pressure. There are two basic ways to define pressure in a nonperiodic MFFA boundary system: The most straightforward way to define pressure in a nonperiodic system is by summing the external boundary contributions F_b over all particles N and dividing it by the total boundary surface A. The external pressure P_{ext} is thus given by

$$P_{ext} = -\frac{1}{A}\sum_{i=1}^{N} F_{b,i} \tag{9}$$

Assuming that the internal mean pressure P_{int} is uniformly distributed throughout the system, $P_{int} = P_{ext}$, and the internal pressure can be obtained using eq 9. However, when there is a net surface tension at the boundary, $P_{int} \neq P_{ext}$, due to the induced Laplace pressure contribution. As the coupling to an external pressure bath will give rise to volume fluctuations, the boundary curvature will also show fluctuations, as $F_b(r_0)$ in eq 2 is dependent on the boundary curvature. Therefore, although the mean field force potential is designed to minimize the net mean surface tension, due to fluctuations in curvature and the (numerical) precision of the MFFA-potential fit itself, a small net surface tension might still occur. For this reason, a more robust way to define the internal pressure based on the work of Schofield and Henderson[39] was used:

$$[p]_{\Omega,int} = \frac{2([K]_\Omega - [\Theta]_{\Omega,int})}{3V_\Omega} \tag{10}$$

In this approach, the internal pressure is given by

$$P_{int} = [p]^{Tr}_{\Omega,int} \tag{11}$$

Equation 10 gives the pressure tensor within every macroscopic subregion Ω. Here, $[K]_\Omega$ is the kinetic energy tensor of the atoms within Ω and $[\Theta]_{\Omega,int}$ is the internal virial tensor. The quantity V_Ω denotes the volume of Ω. For the entire system,

$$V = \frac{4}{3}\pi({R_{out}}^3 - {R_{in}}^3) \tag{12}$$

with R_{out} being the radius of the outer boundary potential and R_{in} being the radius of the inner boundary potential.

Due to the particle interactions with the boundary, the internal virial tensor $[\Theta]_{\Omega,int}$ can be decomposed into two parts:

$$[\Theta]_{\Omega,int} = [\Theta]_{\Omega,int,pairs} + [\Theta]_{\Omega,int,wall} \tag{13}$$

The first part, $[\Theta]_{\Omega,int,pairs}$, results from the direct pair interactions between all particles in the system. The second part, $[\Theta]_{\Omega,int,wall}$, results from the interactions of particles with the boundary.

To obtain the virial contribution coming from the direct pair interactions, $[\Theta]_{\Omega,int,pairs}$, all boundary force contributions acting on atom i are neglected. Therefore, the single sum internal virial tensor $[\Theta]_{\Omega,int,pairs}$ in this nonperiodic system is given by

$$[\Theta]_{\Omega,int,pairs} = -\frac{1}{2}\sum_{i=1}^{N} (\hat{F}_i - \hat{F}_{b,i}) \otimes \hat{r}_i \tag{14}$$

where F_i is the total force and $F_{b,i}$ the boundary force acting on atom i.

The virial contribution coming from the interactions of particles with the boundary $[\Theta]_{\Omega,int,wall}$ is given by

$$[\Theta]_{\Omega,int,wall} = k\sum_{i=1}^{N} F_{b,i} \otimes \hat{\mathbf{r}}_{center,i} d(i) \tag{15}$$

where $\hat{\mathbf{r}}_{center,i}$ is the unit normal factor connecting the center of the spherical system with the particle i and $d(i)$ is the distance to the boundary along $\hat{\mathbf{r}}_{center,i}$. It should be noted that $d(i) > 0$ when the particle is located in the region within the boundaries and $d(i) < 0$ when the particle resides outside of the boundaries. The latter is possible due to the soft nature of the boundary potential. The prefactor k has a value of -1 when summing the contributions coming from the outer boundary and 1 when summing the contributions coming from the inner boundary.

In practice, the calculation of the boundary virial contribution $[\Theta]_{\Omega,int,wall}$ is done within the same single loop as the calculation of the boundary force on each particle.

A convenient and simple way to control the pressure in the system is by coupling to a Berendsen barostat.[38] To maintain the system uniformity and to prevent the buildup of additional pressure inside, for example, a vesicle, the whole system is subjected to isotropic scaling, i.e., scaling both inner and outer radius as well as all atomic coordinates with the same scaling matrix μ. The form of the boundary potentials remains fixed, however. The effect of scaling R on the MFFA potential is negligible for the size of system of interest in this work. For instance, the standard deviation in the effective radius of a pure water system at $T = 323$ K is only about 2% for $R = 10$ nm.

2.4. Simulation Setup. ***CG Model.*** All simulations were performed using the coarse grained (CG) model of Marrink et al.[34] In this model, which is based on the work of Smit et al.,[40] small groups of atoms (four to six heavy atoms) are united into a single interaction center. Water was also modeled as a combined particle representing four real water molecules. In addition to the LJ interactions, a Coulombic potential with a relative dielectric constant of 20 describes the electrostatic interactions between the positively charged choline and the negatively charged phospate beads of the zwitterionic PC head groups. Both the LJ and Coulomb interactions are restricted to short-range interactions only using a shift-based cutoff of 1.2 nm. The lateral density profiles of the membranes obtained using the CG model correspond closely with those obtained from atomistic simulations. For details of the method and its applications, we refer to the original publications.[34,35] On the basis of a comparison of diffusion rates of real water and the CG water, the CG water is found to diffuse 4 times faster. A similar factor was found for lipid systems, suggesting that the relative dynamics using the CG model are well preserved. When comparing the actual simulation time with real times, the simulation time should be scaled by a factor of 4. All timescales presented in this manuscript are still the actual CG timescales.

Pure Water. To test the method and its implementation, a system of pure CG water in a spherical shell with $R_{in} = 10$ nm and $R_{out} = 22$ nm was simulated at a temperature of 323 K and a pressure of 1 bar using the MFFA boundary conditions. The MFFA potentials were calculated using eq 2. The radial distribution function in eq 2 was obtained from an NPT simulation of 1500 CG-water beads under periodic boundary conditions at 323 K and 1 bar. For the cutoff of the MFFA potential, the same values were chosen as those for the normal cutoff of the pairwise interactions, 1.2 nm. Pressure and temperature were coupled to an external bath using the Berendsen coupling method ($\tau_P = \tau_T = 1.0$ ps^{-1}, $\beta = 5 \times 10^{-5}$ bar^{-1}).[38] Both rigid body linear and angular momentum were removed every time step.

Lipid Bilayer. To test any possible effect of the MFFA boundary approach on the bilayer structure, the periodicity along the Z-axis of a periodic bilayer system was removed and replaced by two MFFA boundary potentials. The MFFA boundary potentials were derived for a planar system in a similar way as in eqs 2–6. An equilibrated DPPC bilayer patch consisting of 128 lipids, taken from a conventional simulation under periodic boundary conditions, was placed within the reaction zone of the MFFA boundary system. A CG solvent layer of 2.5 nm thickness was placed between the membrane patch and the MFFA boundaries. Additionally, to test any possible effects on the membrane properties of the antifreeze particles in conjunction with the MFFA method, a solvent consisting of 5% antifreeze particles was used.

TABLE 1: System Setup for Vesicle Simulations

vesicle diameter (nm)	R_{in} (nm)	R_{out} (nm)	# DPPC	# W (CG)
20	2.5	12.5	2528	43303
30	6.0	18.0	5915	140811
40	10.0	22.0	10529	242720
a			5915	298088
b			11354	232820
50	15.5	27.5	18271	374408
60	20.0	32.5	27384	639722

[a] System containing an insufficient number of lipids to form a vesicle. [b] System containing a number of lipids in excess of that required to form a vesicle.

Vesicles. In order to study the formation of vesicles of increasing size, five different systems corresponding to vesicles with diameters of 20, 30, 40, 50, and 60 nm were prepared. The number of lipids required to form the desired vesicle size was estimated from the area per lipid of a CG simulation of a DPPC membrane at 323 K. From the area per lipid (0.64 nm^2) and the lateral phosphate−phosphate distance (4 nm), the required numbers were calculated assuming that the total average area per lipid of both of the monolayers of the vesicle is close to this value; see Table 1. Control simulations in which a greater or lesser number of lipids were used were also performed. The starting configurations were obtained by copying a small cubic periodic box, containing a randomly mixed DPPC/water system, multiple times into a simulation box which embeds the spherical shell of interest. The spherical shell was then cut from the simulation box. To obtain a smooth starting configuration, a maximum of one DPPC tail bead per lipid was allowed to be out of the spherical shell. If this criterion was not fulfilled, then the excess DPPC beads were removed and the remaining beads were converted into CG-water beads. Alternative starting configurations were prepared by removing all lipids within a distance of 2−2.5 nm from the boundary so that a layer of pure solvent surrounded the lipid solution. During the simulations, the lipids were subjected to either the same MFFA boundary potential as the water (nonselective) or to a purely repulsive potential (selective). This repulsive potential was harmonic in nature and was intended to bias the diffusion of the lipids toward the central zone, thus enhancing the rate of vesicle formation.

Spontaneous Aggregation. As a control, the structural properties of the vesicles formed using the MFFA boundary approach were compared to the structure of vesicles formed by using the spontaneous aggregation of lipids in a fully periodic system. To this end, the simulation of the 20 nm vesicle (Table 1) was also performed in a 28 nm cubic periodic box at the same state point but with 2528 DPPC lipids randomly distributed within a sphere of 13 nm radius. The remaining volume in the box was filled with CG water. This simulation was performed in duplicate starting from different lipid distributions.

Artificial Pores. In a similar fashion to the spherical MFFA approach, cylindrical shaped boundaries were also implemented. By restraining the carbon tails in the lipids, these boundaries were used to induce pores inside the membrane of any chosen size.[41] When the restraining force has both repulsive and attractive contributions, a pore is formed in which the carbon tails are forced to form the interface of the pore (hydrophobic pore). Due to its hydrophobic nature, such a pore is energetically unfavorable; however, the edge tension induced at the pore interface is compensated by the attractive contribution from the potential. When only repulsive contributions are present, the membrane is free to choose its most favorable pore structure.

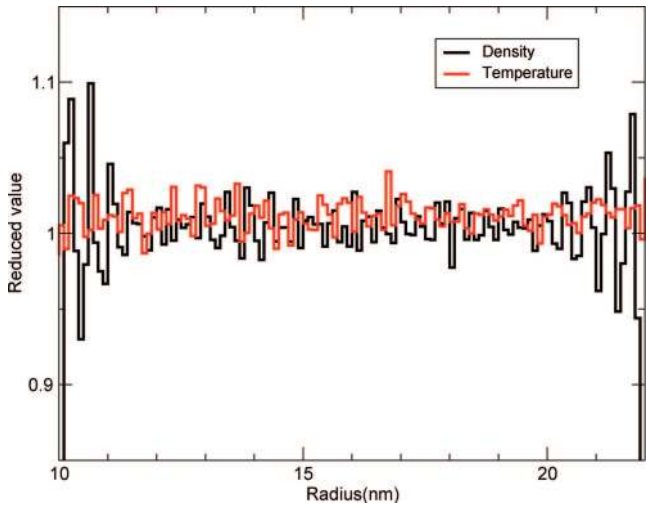

Figure 3. A plot of the temperature and density distribution throughout the simulation shell for a pure CG-water system at 323 K in the NPT ensemble. Relative values are given with respect to the reference values of conventional MD in the same ensemble.

In the case of DPPC (CG model), when the restraining radius on the tails is greater than 1.2 nm, the interface of a pore is completely formed by the lipid head groups (hydrophilic pore). In such a pore, the lipids can freely exchange (flip-flop) between the two monolayers, allowing the membrane to equilibrate. Using this approach, several pores can be induced in the liposome while still conserving its curvature and shape. In this way, a metastable liposome is able to relax to its lowest thermodynamical state. Moreover, the ratio in flip-flops between the two monolayers provides a useful criterion to determine the state of equilibrium of a given vesicle.

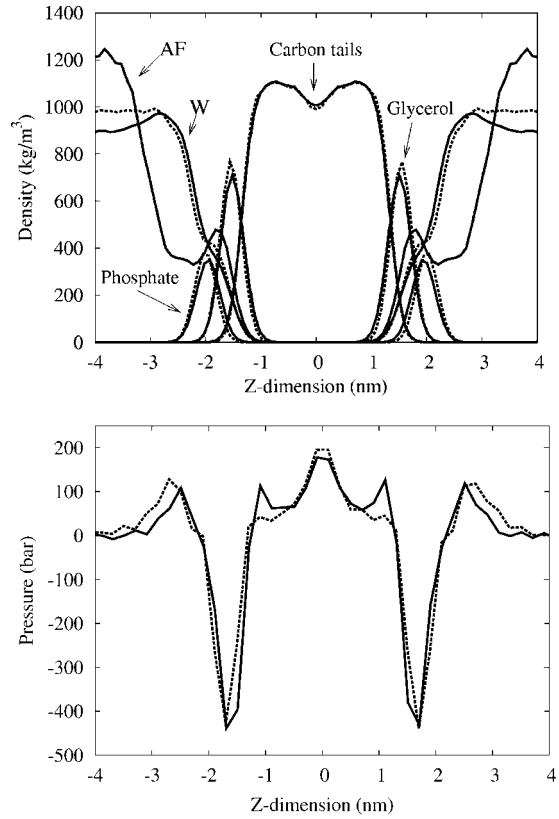

Figure 4. Plot of the lateral density and pressure profile in the bilayer simulated under periodic boundary conditions (conventional setup) or MFFA boundary potentials in addition to antifreeze particles (boundary setup). Thick lines represent the boundary setup, and thin lines, the conventional setup. The peaks of water (W) and antifreeze (AF) particles in the boundary setup are scaled with respect to their relative density.

3. Results

3.1. Test Case: Pure Water. Figure 3 shows the density and temperature profile for a 10 ns simulation of pure CG water at 323 K in the NPT ensemble using MFFA boundary potentials at $R_{in} = 10$ and $R_{out} = 22$ nm. While some ordering in the density profile is evident near the boundary, this fades within 2 nm of the boundary, giving the normal isotropic bulk properties. Therefore, to diminish artifacts at the edges of the reaction zone of interest, the width of the buffer zone is ideally >2 nm. The density in the reaction zone is in good agreement with conventional MD simulation of CG water.

3.2. Test Case: Lipid Bilayer. Figure 4 shows the comparison of the lateral density and pressure profile for a 128-lipid DPPC bilayer under periodic boundary conditions with "pure" CG water (conventional setup) or under MFFA boundary conditions with the addition of 5% antifreeze particles (boundary setup). Figure 4 demonstrates that, apart from some minor differences, both the pressure and density profiles obtained with the boundary setup are in good agreement with the results obtained with the conventional setup. The minor differences are related to the presence of the antifreeze particles rather than the presence of the MFFA boundaries. The bilayer profiles obtained without the antifreeze particles are almost indistinguishable between the boundary and conventional setup (data not shown). Comparison of the distribution of the relative densities for normal and antifreeze water reveals that the antifreeze particles are somewhat repelled from the interface. Although one could, in principle, further fine-tune the interactions between antifreeze particles and the particle types constituting the bilayer in order to obtain a more homogeneous distribution, this is not desirable. The main purpose of the antifreeze particles is to prevent freezing of the water phase which is nucleated by the ordering effect of the boundary (compare to Figure 3). The increased relative density of the antifreeze particles in the bulk water slab is therefore only advantageous. The pressure profile shows a remarkable feature, namely, the appearance of two small shoulders ($z = \pm 1$ nm) to the big positive peak arising from the carbon tails. Interestingly, similar shoulder peaks are also more pronounced in the pressure profiles of atomistic DPPC bilayers.[42] Although we do not understand the origin of this effect, the addition of antifreeze particles appears to result in a more realistic stress distribution across the bilayer. We also evaluated the effect of the system setup on the lateral diffusion rates of the lipids, and found it to be very small. In the boundary setup, the lateral diffusion constant increases $3 \pm 1\%$ compared to the conventional simulation setup. In conclusion, within the resolution obtained by our coarse grained model, these small changes in structural and dynamic properties when using the boundary setup are negligible.

3.3. Application: Vesicle Formation. The ability to form vesicles using the MFFA boundary approach was tested using different approaches to generate the starting structure and to accelerate the demixing of lipids and water. In the simulations where only the MFFA boundary potential of the CG water was used, the lipids condensed into patches on the boundary surface within a few nanoseconds. Depending on the concentration, the lipids either formed interpenetrating networks between the boundaries (high or desired concentration regime (Table 1)) or

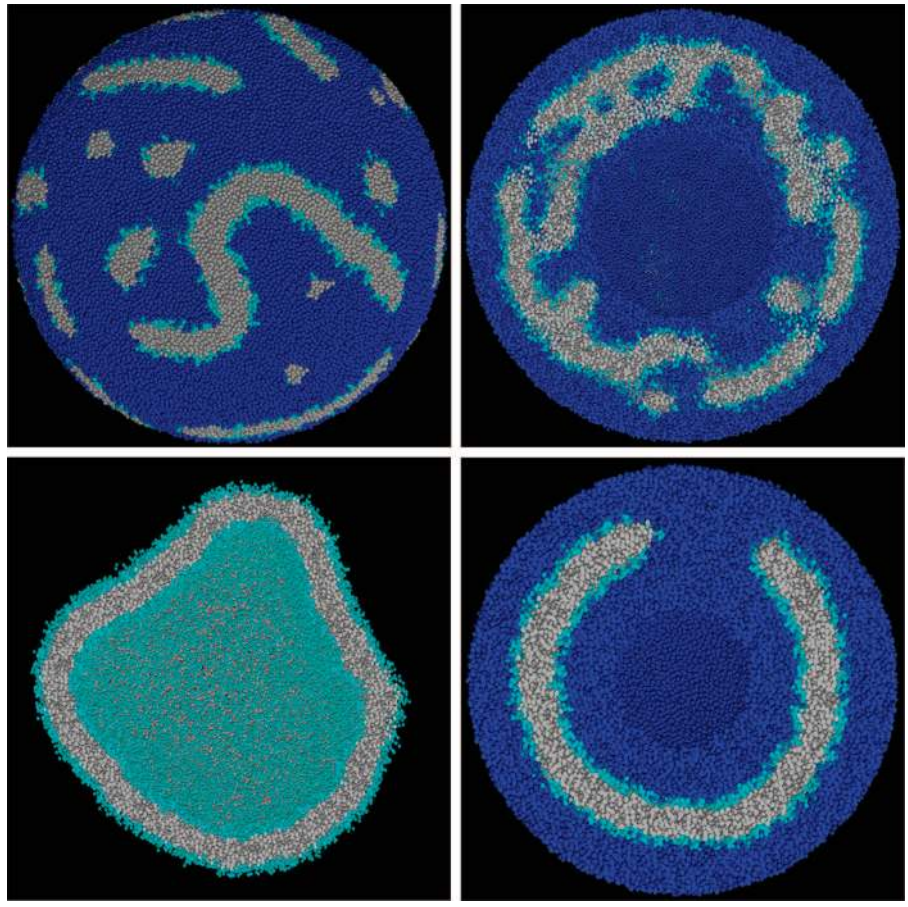

Figure 5. Examples of cases in which DPPC vesicles failed to form under various conditions. The head groups are colored cyan, the tail groups are grey, and the water is blue. (upper left) Top view of a 40 nm system simulated under MFFA boundary conditions without either a selective repellent potential or an additional water layer. Clear patch formation is observed at the surface of the boundaries, and the configuration becomes kinetically trapped. (upper right) Cross section of the formation of a 40-nm-diameter vesicle. An additional harmonic potential of 0.3 nm width and a force constant of 50 kJ mol^{-1} nm^{-2} was used to enhance demixing of the lipids at the boundary interface. The width of the repellent potential was insufficient to cause a "molding" effect. The snapshot reveals widespread lipid patch formation through the system after 50 ns of simulated time. (lower left) Cross section of a 40-nm-diameter vesicle formed from an excessive lipid amount. The simulation was started with an additional CG-water layer at the boundary of 2.0 nm thickness to prevent condensation of lipids at the boundaries. The snapshot shows a floppy irregular shaped vesicle sealed after 8 ns of simulated time. (lower right) Cross section of a 30-nm-diameter vesicle formed from an insufficient amount of lipids. A snapshot after 14 ns of simulation reveals the presence of a large pore (around 6 nm in diameter).

condensed as a monolayer on one of the boundaries in the lower concentration regime. None of the attempts resulted in the formation of a complete vesicle within 50 ns (Figure 5). The failure of vesicles to form could be due to a number of reasons. One possibility is that the width of the region in which lipids and water were randomly mixed initially was too wide. This, especially in the case of larger systems, could lead the lipids to become trapped in kinetic intermediates, such as those shown in Figure 5. In this case, the "molding" effect of the repulsive potential was insufficient, resulting in widespread lipid patch formation and double lamellar vesicles full of pores and interlamellar stalks. An excessive or insufficient number of lipids also resulted in the formation of irregularly shaped aggregates (Figure 5). In cases where there were an excessive number of lipids, very floppy, irregular-shaped vesicles were formed. Where the amount of lipid was insufficient, nearly perfect spherical vesicles containing one or more pores were obtained. In this case, pore closure was not possible, as the inner boundary potential prevented further shrinkage.

Spherical and sealed vesicles could however be formed by either excluding lipids in the starting structure from a solvent shell of 2−2.5 nm thick or applying a repulsive boundary potential to the lipids with a force constant exceeding 10 kJ mol^{-1} nm^{-2} and a width of 1.5−2.0 nm. Using this approach, vesicles form quickly (Figure 6). The time scales required ranged from 6 ns for a 20 nm vesicle to 10−20 ns for the largest vesicles of 60 nm diameter. Figure 7 shows the five DPPC vesicles formed using this method. The largest of these vesicles was 60 nm in diameter and was composed of 27384 lipids, approximately 3 times the smallest size observed experimentally.

3.4. Application: Vesicle Equilibration. In order to compare the structure of the vesicles formed under MFFA boundary conditions to a vesicle formed under standard periodic boundary conditions (Marrink et al.[4]), the lateral density profiles with respect to the center of the vesicle were compared (see Figure 8). The lateral density profiles seem similar for the vesicles obtained using the two methods. The maximum deviation between the profiles is in the order of 0.3 nm. Such deviations can both be due to shape fluctuations and to variations within the spontaneously formed vesicles arising from a difference in the distribution of lipids between the two leaflets. Although the comparison is not statistically rigorous, Table 2 suggests that the variation in the lipid distribution over the membrane leaflets from the vesicles obtained with the MFFA boundary approach is similar to the distribution within vesicles formed under periodic boundary conditions. However, based on these results, it is not possible to say what would be the true equilibrium distribution. Once sealed, lipid flip-flops are not observed even

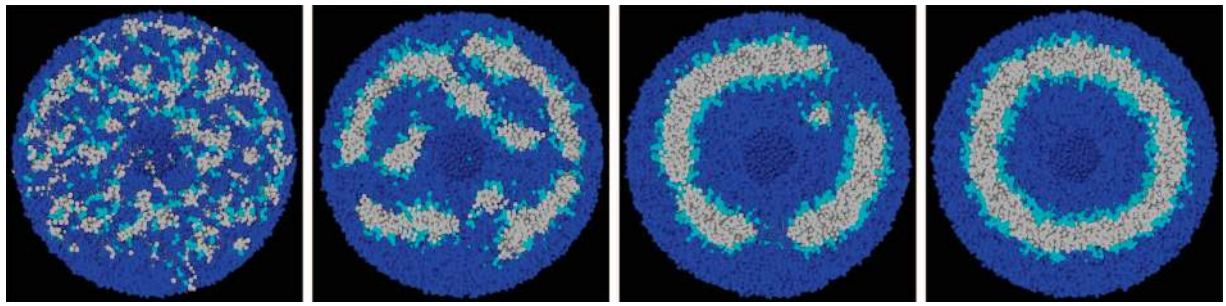

Figure 6. Vesicle formation of a 20-nm-diameter pure DPPC vesicle. An additional repulsive harmonic potential of 0.3 nm width and a force constant of 50 kJ mol^{-1} nm^{-2} was used to enhance demixing of the lipids at the boundary interface. Snapshots are shown at $t = 0$, 1, 5, and 8 ns. The head groups are colored cyan, and the tail groups, grey. A contour of the 2.5-nm-radius internal cavity is visible.

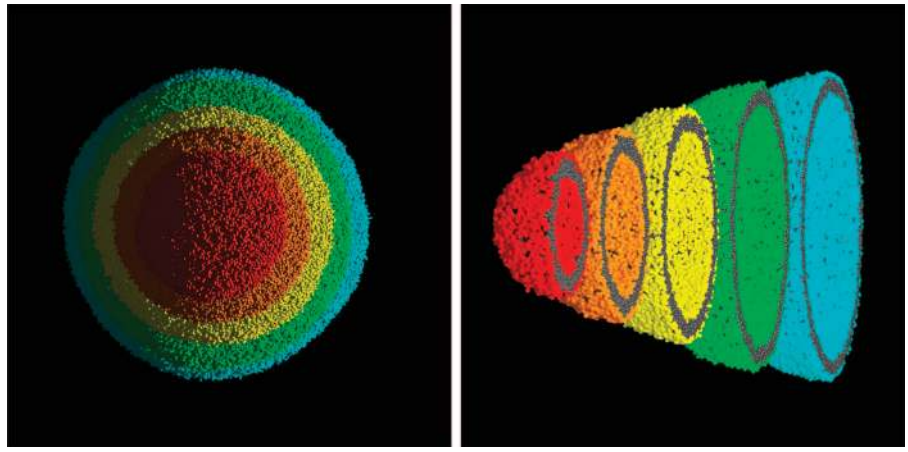

Figure 7. Overview of the five different vesicles formed by the presented MFFA boundary method. Shown from front to back are 20-, 30-, 40-, 50-, and 60-nm-diameter pure DPPC vesicles.

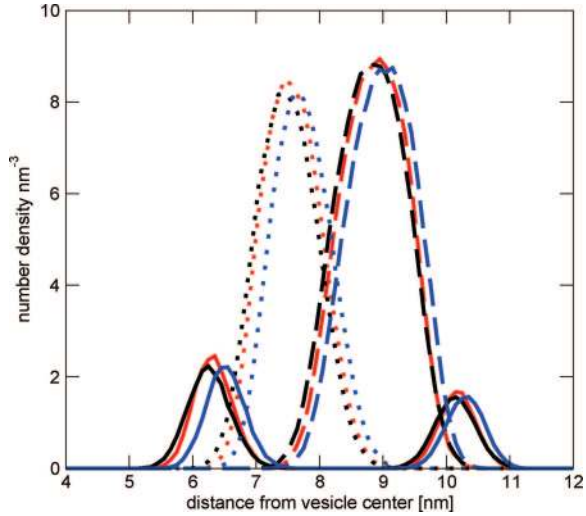

Figure 8. The radial number density in the membrane with respect to the center of the vesicle. The red lines represent the vesicle obtained by Marrink et al.[4] Black and blue lines represent two vesicles formed under MFFA boundary conditions. Solid lines represent the head group region. Dotted lines represent the tail regions of the inner monolayer, and dashed lines, the tail region of the outer monolayer.

on a microsecond time scale, preventing further equilibration of the vesicles. In order to resolve this issue, artificial pores were introduced into the vesicle. To achieve this, a purely repellent cylindrical potential with a force constant of 50 kJ mol^{-1} nm^{-2} and a radius of $R = 1.8$ nm diameter was used. This potential was only felt by the carbon tails of the lipids and was present from the start of the simulation. A vesicle formed within 10 ns, similar to the previous results, but which

TABLE 2: Comparison of Boundary Approach with Conventional Spontaneous Aggregation (Shown Is the Number of DPPC Molecules in the Inner and Outer Leaflet of the Membrane)

	# $DPPC_{in}$	# $DPPC_{out}$
Marrink et al.:[4]	940	1588
conventional aggregation (I):	940	1588
conventional aggregation (II):	912	1616
MFFA boundary (I):	921	1607
MFFA boundary (II):	923	1605

contained two hydrophilic pores. This simulation was continued for 120 ns to allow for the equilibration between the two leaflets. The results are shown in Figure 9. Figure 9A shows the fluctuation in the number of lipids in the inner monolayer resulting from flip-flops between the inner and outer monolayer. Figure 9B reveals the time averaged distribution in the monolayer population. On the basis of this distribution, we estimated that there would be around 935 lipids in the inner monolayer and 1593 lipids in the outer monolayer at equilibrium. These results suggest that the values obtained with the "stand-alone" MFFA boundary method presented in Table 2 are within the tails of the expected distribution. From Figure 9A, it appears that the number of flip-flop events between the two monolayers stabilizes after approximately 30 ns. Therefore, the mismatch between the values obtained by the "stand-alone" MFFA boundary method is most likely related to an insufficient relaxation time during the formation of the vesicle. However, the introduction of artificial pores is a simple and powerful method to obtain equilibrated vesicles.

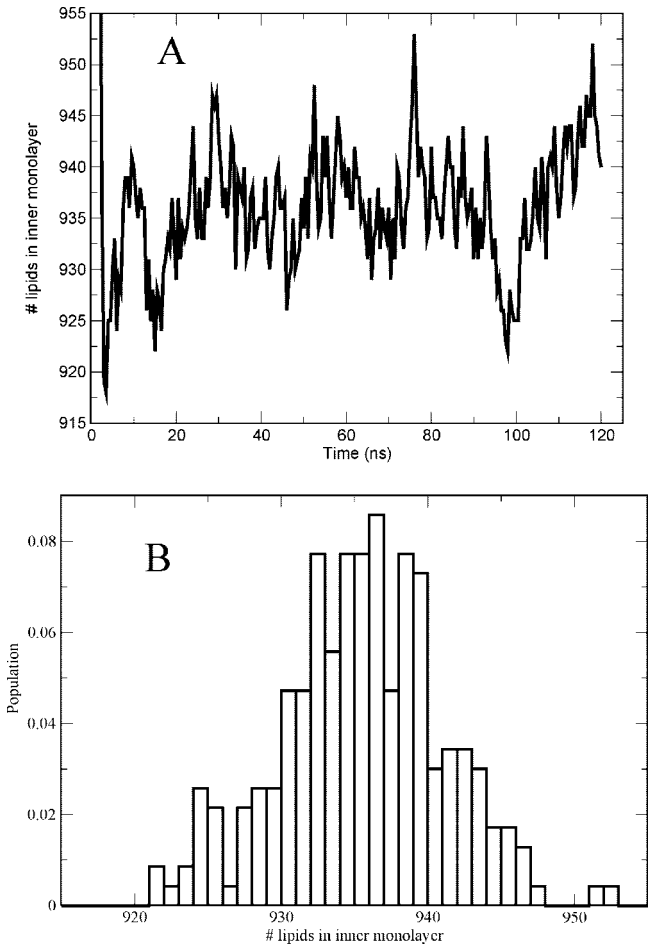

Figure 9. (A) Number of lipid molecules in the inner monolayer as a function of time in a DPPC vesicle (2528 lipids, 323 K). (B) Distribution of lipids in the inner monolayer averaged over time (120 ns).

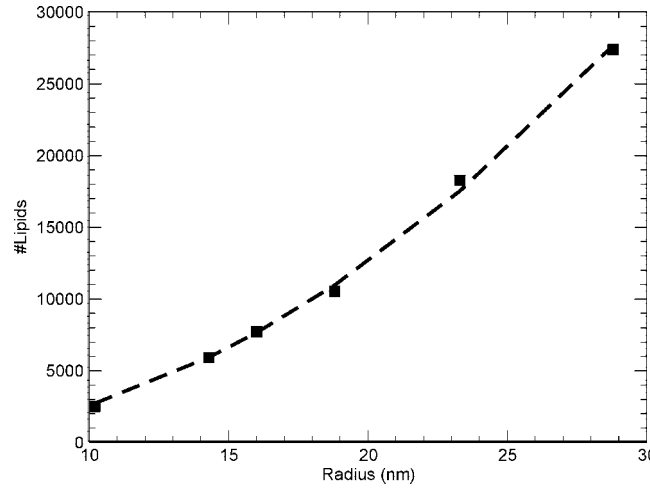

Figure 10. Total number of DPPC lipids versus vesicle radius for vesicles obtained from the simulations (black squares). The radius was calculated from the average distance of the phosphate groups in the outer monolayer to the center of the vesicle. The dashed line is a fit of eq 16. Here, $A = 0.654$ nm and $d = 4.061$ nm.

4. Discussion

Our aim was to develop an approach that allows large-scale simulations of vesicular systems, without compromising on the relevant near-atomic details of the underlying coarse grained model. The results show that the use of a boundary potential to replace bulk solvent, both inside and outside the vesicle, is reasonable. Comparison of the structure of both lamellar bilayers and of vesicles obtained with the boundary method to those obtained using full solvation revealed no significant artifacts as long as the solvent shell was sufficiently large. A solvent shell of 2.5 nm was found to be sufficient for the effect of the boundary potential to be negligible.

As expected from a model based on a cutoff scheme to evaluate the pair interactions, the gain in computational efficiency is found to be approximately linear with respect to the relative decrease in solvent particles. This in turn depended on vesicle size, eq 1. For the vesicle of 60 nm in diameter, the gain in computational efficiency was considerable, around 60% in comparison with the same vesicles under normal cubic periodic boundary conditions. For more complex periodic boxes such as the rhombic dodecahedron, the gain in efficiency was approximately 45%. The boundary method will become progressively more effective for larger vesicles. Considering, for instance, a vesicle of 100 nm, the gain in computational efficiency is estimated as 72% compared to a cubic box and 60% for a rhombic dodecahedron. In practice, the estimated efficiency gain will be even higher as perfect linear scaling of computational speed with the number of solvent particles was assumed, which is never achieved in practice. The additional computational costs due to the implementation of the MFFA boundary are small. This is because the boundary force can be tabulated as a set of cubic splines which are only dependent on the position of the particles within the system. In GROMACS-3.3, the additional costs due to the implementation of the MFFA boundary method were less than 1% of the total computational cost.

Further speed-up is obtained for the formation of the vesicles, due to the molding effect of the boundary potentials. While one could start from preassembled vesicles, it should be noted that for a vesicle of a given radius neither the total number of lipids nor the ratio between the lipids in the inner and outer monolayer are known precisely. As a result, preassembled vesicles are likely to be in a state of stress. Using the self-assembly approach, stress can be released through the optimization of the vesicle size and the exchange of lipids between the monolayers during the process of vesicle formation. Moreover, we have demonstrated that artificial pores can be used to allow further equilibration even after the vesicles have sealed. This method seems essential to obtain and to ensure fully equilibrated vesicles.

Our results indicate that the best method for vesicle formation is obtained if a layer of water surrounds the lipid solution in the starting configuration. This approach appears preferable to the method where a selective repulsive potential is used for the lipids. First, the solvent shell is easier to implement; second, the formation of vesicles is faster, especially for larger vesicles (>30 nm diameter). The reason for this is that, in the case of the selective repulsive potential method, the diffusion toward the reaction zone becomes the rate determining step in the vesicle formation. A prerequisite of the method presented is that the total number of lipids required is approximately known. An over- or underestimation of the number of lipids required may lead to the formation of stressed vesicles, as shown in Figure 5. The appropiate number of lipids can be estimated from the following equation:

$$f(r) = \frac{4\pi}{A}((r-d)^2 + r^2) \qquad (16)$$

Here, $f(r)$ is the total amount of lipids in the vesicle as function of its radius r, A is the area per lipid, and d is the characteristic thickness of the bilayer. A fit of our results to eq 16 is given in Figure 10. From Figure 10, it should be noted that a simple prediction based on a fixed average area per lipid ($A = 0.654$

nm^2) and thickness ($d = 4.06$ nm) from a bilayer patch closely reproduces the data obtained for vesicles over the whole size range. This result might be surprising given that the difference in area per lipid between the two monolayers is relatively large (±30%) in the lower regions of the fitted curve.

Potential applications of the boundary potential method are diverse. We have shown that the method is a fast way to efficiently generate equilibrated vesicles. In addition, for a given minimum width of the solvent layer, the use of a spherical boundary is recommended to avoid artifacts caused by an otherwise inhomogeneous solvent distribution around the vesicle when simulated under periodic boundary conditions. Due to the reduction in solvent degrees of freedom, the boundary approach in general allows the study of extended length and time scales for vesicular membranes. Especially for large vesicles, the gain in computational speed is very substantial. Formation of nanodomains, for instance, is currently being simulated in our group for systems of comparable size to those used in experimental studies. The MFFA approach is also flexible; increasing the volume enclosed by the boundary potentials allows one to include peptides or proteins. Membrane poration by antimicrobial peptides is an example of a process which would highly benefit from using our spherical boundary method, taking place in a small solvent shell surrounding the bilayer. For the size of the vesicles formed in this paper, thermal deformations are expected to be very small.[43] For larger or softer vesicles, these modes will become more important. In such a case, an increase in the width of the solvent shell may be required to prevent suppression of such undulations. In the case of mixed systems, where the effective area per molecule is not known, an increase in the width of the solvent layers might also be required to guarantee a greater flexibility for the preferred size of self-assembling vesicles. Furthermore, one could study fusion of two vesicles by removing the outer boundary potential (although for the complete fusion pathway also the inner boundary potentials would have to be removed). Another advantage of the method is its possibility to increase the internal pressure inside the vesicle, by separate scaling of the inner and outer boundaries. Osmotic shock experiments could thus be simulated. Finally, spherical boundary potentials could be applied to reduce the solvent layer around other molecules or molecular assemblies with (quasi-)spherical geometry, such as proteins, polymer chains, and micelles.

5. Conclusions

A method has been presented to efficiently simulate the properties of self-assembled vesicles at near-atomic detail. The method involves the application of boundary potentials to replace both the internal and external excess bulk solvent. Vesicles with diameters in the range from 20 to 60 nm were obtained on a nanosecond time scale, without any noticeable effect of the boundary potentials on their structure. Moreover, a powerful method for equilibration of vesicles by introducing artificial pores was demonstrated. These detailed vesicles may be subjected to further studies including phase separations and osmotic shock simulations.

Acknowledgment. We would especially like to acknowledge Prof. H. J. C. Berendsen and Samuli Ollila for the useful discussions. We thank the MtC (Molecule to Cell) project of NWO for the financial support. Acknowledgment is also made to the HPC cluster facilities of the University of Groningen for providing CPU time. Finally, we would like to thank our colleague Dr. Tsjerk Wassenaar for the artistic pictures of vesicles included in this paper.

References and Notes

(1) Drouffe, J.; Mags, A. C.; Leibler, S. *Science* **1991**, *254*, 1353–1356.
(2) Noguchi, H.; Takasu, M. *Phys. Rev. E* **2001**, *64*, 41913.
(3) Yamamoto, S.; Maruyama, Y.; Hyodo, S. *J. Chem. Phys.* **2002**, *116*, 5842–5849.
(4) Marrink, S. J.; Mark, A. E. *J. Am. Chem. Soc.* **2003**, *125*, 15233–15242.
(5) Stevens, M. J.; Hoh, J. H.; Woolf, T. B. *Phys. Rev. Lett.* **2003**, *91*, 188102.
(6) Smeijers, A. F.; Markvoort, A. J.; Pieterse, K.; Hilbers, P. A. *J. Phys. Chem. B* **2006**, *110*, 13212–13219.
(7) Shillcock, J. C.; Lipowsky, R. *Nat. Mater.* **2005**, *4*, 225–228.
(8) Wang, Z. J.; Frenkel, D. *J. Chem. Phys.* **2005**, *122*, 234711.
(9) Cooke, I. R.; Deserno, M. *J. Chem. Phys.* **2005**, *123*, 224710.
(10) Brannigan, G.; Brown, F. L. H. *J. Chem. Phys.* **2004**, *120*, 1059–1071.
(11) Kasson, P. M.; Kelley, N. W.; Singhal, N.; Vrljic, M.; Brunger, A. T.; Pande, V. S. *Proc. Natl. Acad. Sci. U.S.A.* **2006**, *103*, 11916–11921.
(12) Laradij, M.; Kumar, P. B. S. *J. Chem. Phys.* **2006**, *123*, 224902.
(13) de Vries, A. H.; Mark, A. E.; Marrink, S. J. *J. Am. Chem. Soc.* **2004**, *126*, 4488–4489.
(14) Knecht, V.; Marrink, S. J. *Biophys. J.* **2007**, *92*, 4254–4261.
(15) Cronell, B. A.; Fletcher, G. C.; Middlehurst, J.; Separovic, F. *Biochim. Biophys. Acta* **1982**, *690*, 15–9.
(16) Marrink, S. J.; Mark, A. E. *J. Am. Chem. Soc.* **2003**, *125*, 11144–11145.
(17) Biltonen, R. L.; Lichtenberg, D. *Chem. Phys. Lipids* **1993**, *64*, 129–142.
(18) Koynova, R.; Caffrey, M. *Biochim. Biophys. Acta* **1998**, *1376*, 91–145.
(19) Marrink, S. J.; Risselada, H. J.; Mark, A. E. *Chem. Phys. Lipids* **2005**, *135*, 223–244.
(20) Ayton, G.; Smondyrev, A. M.; Bardenhagen, S. G.; McMurtry, P.; Voth, G. A. *Biophys. J.* **2002**, *83*, 1026–1038.
(21) Sevink, G. J. A.; Zvelindovsky, A. V. *Macromolecules* **2005**, *38*, 7502–7513.
(22) Lyubartsev, A. P. *Eur. Biophys. J.* **2005**, *35*, 53–61.
(23) Wassenaar, T. A.; Mark, A. E. *J. Comput. Chem.* **2006**, *27*, 316–325.
(24) Berkowitz, M.; McCammon, J. A. *Chem. Phys. Lett.* **1982**, *90*, 215.
(25) Brooks, C. L., III; Karplus, M. *J. Chem. Phys.* **1983**, *79*, 6312–6325.
(26) Brünger, A. T.; Brooks, C. L., III; Karplus, M. *Chem. Phys. Lett.* **1984**, *105*, 495–500.
(27) King, G.; Warshel, J. *J. Chem. Phys.* **1989**, *91*, 3647.
(28) Rullmann, A. C.; van Duijnen, P. T. *Mol. Phys.* **1987**, *61*, 293–311.
(29) Juffer, A. H. On the modelling of solvent mean force potentials. Ph.D. Thesis, University of Groningen, The Netherlands, 1993.
(30) Beglov, D.; Roux, B. *J. Chem. Phys.* **1994**, *100*, 9050–9063.
(31) Yuhui, L.; Krilov, G.; Berne, B. J. *J. Phys. Chem. B* **2005**, *109*, 463–470.
(32) Heller, H.; Schaefer, M.; Schulten, K. *J. Phys. Chem.* **1993**, *97*, 8343–8360.
(33) Bolterauer, C.; Heller, H. *Eur. J. Biochem.* **1996**, *24*, 322–334.
(34) Marrink, S. J.; de Vries, A. H.; Mark, A. E. *J. Phys. Chem. B* **2004**, *108*, 750–760.
(35) Marrink, S. J.; Risselada, H. J.; Yefimov, S.; Tieleman, D. P.; de Vries, A. H. *J. Phys. Chem. B* **2007**, *111*, 7812–7824.
(36) Van der Spoel, D.; Lindahl, E.; Hess, B.; Groenhof, G.; Mark, A. E.; Berendsen, H. J. C. *J. Comput. Chem.* **2005**, *26*, 1701–1718.
(37) Eichinger, M.; Heller, H.; Grubmüller, H. In *EGO -An efficient molecular dynamics program and its application to protein dynamics simulations*; World Scientific: Singapore, 2000.
(38) Berendsen, H. J. C.; Postma, J. P. M.; van Gunsteren, W. F.; Di Nola, A.; Haak, J. R. *J. Chem. Phys.* **1984**, *81*, 3684–3690.
(39) Schofield, P.; Henderson, J. R. *Proc. R. Soc. London, Ser. A* **1982**, *379*, 231–246.
(40) Smit, B.; Hilbers, P. A. J.; Esselink, K.; Rupert, L. A. M.; Van Os, N. M.; Schlijper, A. G. *J. Phys. Chem.* **1991**, *95*, 6361–6368.
(41) Tolpekina, T. V.; den Otter, W. K.; Briels, W. J. *J. Chem. Phys.* **2004**, *121*, 12060–12066.
(42) Ollila, S.; Hyvonen, M. T.; Vattulainen, I. *J. Phys. Chem. B* **2007**, *111*, 3139–3150.
(43) Lipowski, R.; Sackmann, E. *Structure and Dynamics of Membranes: from Cell to Vesicle*; Elsevier: North-Holland, Amsterdam, 1995.

JP0758519